The Astrophysical Journal, 893:40 (7pp), 2020 April 10 https://doi.org/10.3847/1538-4357/ab7db6


# Quasiperiodic Velocity Fluctuations in Eruptive Prominences Observed by AIA/SDO

Tsvetan Tsvetkov and Nikola Petrov
Institute of Astronomy and National Astronomical Observatory, Bulgarian Academy of Sciences, 72 Tsarigradsko shose Blvd., 1784 Sofia, Bulgaria
tstsvetkov@astro.bas.bg
*Received 2019 August 30; revised 2020 March 5; accepted 2020 March 6; published 2020 April 14*

## Abstract

The current study presents an investigation of the behavior of prominences during eruptions. Variations in the distribution of their velocities are detected at altitudes $<0.6\,R_{\odot}$. Detailed analyses are carried out for 304 Å Solar Dynamics Observatory/Atmospheric Imaging Assembly (SDO/AIA) observations. To track the behavior of prominences during eruptions, 41 events in the period 2010–2017 are studied. To follow the rise of a filament on higher altitudes (up to $32\,R_{\odot}$), Solar and Heliospheric Observatory/Large Angle and Spectrometric Coronagraph (SOHO/LASCO) data are also inspected. They are used to obtain kinematic profiles of eruptions. Obtained height–time and speed–time plots of the eruptions show velocity fluctuations in 83% of the explored cases, detected only in the SDO/AIA field of view, and not in any of the prominences observed at higher altitudes by SOHO/LASCO. Time intervals between fluctuations and heights at which they are detected are estimated. Strong periodicity cannot be determined.

*Unified Astronomy Thesaurus concepts:* Solar prominences (1519); Solar filament eruptions (1981)

## 1. Introduction

Eruptive prominences (EPs) are an observational manifestation of processes that take place at coronal magnetic fields. They are assumed to be an outcome of the eruption of large-scale magnetic structures closely related to magnetic inversion lines (Rompolt 1984). The cool and dense prominence plasma remains "frozen" in the surrounding magnetic structure that determines its behavior ($\beta_{\rm prom} < 1$).

EPs are emphasized with large radial (heliocentric) velocity components directed oppositely to the Sun. The typical eruption evolution consists of three stages: a pre-eruptive phase of activation, an acceleration phase, and an eruptive phase with constant or gradually increasing speed (Vrsnak 1998). EPs often exhibit ejection of material during the final stages. In the case where only part of its body is being ejected, the other part may fall back down to the solar surface or continue its existence above the limb (Gilbert et al. 2007b). EPs may first appear as quiescent prominences or as active region ones that erupt due to destabilization processes.

Prominences tend to lie above the magnetic inversion lines (MILs) on the boundary between photospheric regions with opposite magnetic polarity (Babcock & Babcock 1955). The MILs overlap with filament channels (Berger 2012). According to the modern understanding there are four type of MILs that define the overlying prominences (Mackay et al. 2008): the internal bipolar region filament, external bipolar region filament, internal/external bipolar region filament, diffuse bipolar region filament.

According to their geometry and large-scale motions during eruption, prominences can be divided into symmetric and asymmetric (McCauley et al. 2015). The first group usually have a typical arched shape composed of a plurality of fine fibers that are often twisted or interlaced. During eruptions, the arches rise and expand, remaining visible in $H_{\alpha}$ until the end of the eruption when they quickly fade and disappear. Usually the symmetric EPs are situated in the lower part of the large-scale magnetic structure of the associated coronal mass ejection (CME) (Rompolt 1990).

The asymmetric EPs tend to have a similar shape to the symmetric ones at the very beginning of the eruption. Soon they are transformed as one of the legs of the arch breaks away from the surface while the other one remains anchored to the Sun.

It is believed that symmetric EPs are more common (48%) than asymmetric ones (38%) with 14% undefined, although if we consider only polar filaments, the asymmetric ones become more frequent—45% to 39% with 16% undefined (McCauley et al. 2015).

By focusing not on the prominences but on the eruptive process itself, another observational classification divides the eruptions into three classes—full, partial, and confined according to the place in the large-scale magnetic system where magnetic reconnection occurs (Gilbert et al. 2007a). The observational signature of the eruption type is given by the amount of prominence material that is being ejected. Studying the height of a point at which the prominence breaks and part of it may separate from the main body, Gilbert et al. (2000) noticed a clearly expressed maximum of the distribution at an altitude of $1.26R_{\odot}$.

Fluctuations of the velocity of EPs are presented in this paper. Observational data used are described in Section 2 and the results are summarized in Section 3. A brief discussion on possible reasons that cause the fluctuations is included in Section 4. Finally, excepting the kinematic properties, Table A1 in the Appendix provides details about types, classes, and associated phenomena for the explored sample of prominences.

## 2. Observations and Data Processing

Two space-based telescopes are used as the main source of observational data. In addition to their high precision and incessancy, they provide the ability to track the eruptions up to $32\ R_{\odot}$.

To track the behavior of EPs at heights $<0.6\ R_{\odot}$, data from the Atmospheric Imaging Assembly (AIA) instrument on board the Solar Dynamics Observatory (SDO) are used (Pesnell et al. 2012).

He II 304 Å images with an average cadence of about 5 minutes taken with a spatial resolution ~1.″5 (Lemen et al. 2012) are analyzed. Active regions (ARs) are associated using AIA 1600, 1700, and 4500 Å data.

In case the explored eruption continues after the prominence leaves the AIA field of view, data from the Large Angle and Spectrometric Coronagraph/Solar and Heliospheric Observatory (LASCO/SOHO) are inspected (Domingo et al. 1995). Two of the coronagraphs of the LASCO instrument—C2 and C3—allow observations with fields of view from 2–6 $R_\odot$ and 3.7–32 $R_\odot$, respectively. Their average temporal resolution is 12 minutes.

Since the structures of EPs are complex and there is often no coherent leading edge, measurements of the kinematic properties of EPs require accurate determination of the highest part of the prominence, its position, and its tracking during the eruption. For data analysis we obtained an IDL procedure based on the SolarSoftware package (Bentely & Freeland 1998). It includes several steps to fulfill the measurements: (1) primary processing of the images (defective pixels and flat-field correction, heating noise, and cosmic rays impact reduction) and choosing the optimal way to display every image; (2) plotting the mean signal profile from a chosen highest point and the ambient ±3 lines; (3) zooming the plot near the prominence–background boundary and defining the background signal part of the curve; and (4) calculating the mean background signal and standard deviation. Our measurements show that the background signal lies in a range between 0.6–3.8 with a standard deviation of 0.3–2.0. The three times standard deviation interval around the mean value of the signal is used to plot the average signal profile in order to distinguish between the background noise and the prominence signal close to the edge of the filament, where the most diffusive structures of the EP skeleton are usually located . Finally, the procedure defines the prominence–background signal boundary to determine the highest point of the EP and to estimate the measurement error. The final result is then subject to visual inspection since the measured highest point is displayed on the AIA image.

The main advantages of the procedure are the accurate determination of the highest part of the EP, reducing the possibilities of subjectivity, and estimation of measurement error (equal to half of the distance between the chosen point of the EP and its nearest point of the background on the signal profile). Due to the complex structure of EPs and the variety of shapes, twists, and changes of direction they undergo, we measured and freely selected the highest points of the prominence in various images at various (not the same) position angles. We unambiguously estimate the radial distancing of the highest prominence fragment, computing the border point prominence plasma background signal. The position angle is changing with the instantaneous physical alterations of the erupting plasma. To confirm the results, we selected a limited number of events that permit tracking of a same fragment for the whole eruption (or sufficient part of it) and repeated the measurements. In this paper we present the measurements obtained with various points because they offer a longer period of investigation (e.g., a bubble of EP may be visible for only half of the eruption) and the method is universal (the same method is used for every prominence).

To analyze the fluctuations we plotted height–time $h(t)$ and speed–time $v(t)$ plots of eruptions. The height $h$ (the radial distance between the apex of the EP and the solar limb), as well as the absolute error $\Delta h$, is measured directly from observational data. The instantaneous velocity (the projection of the EP velocity onto the plane of the sky) is determined using the data from two consecutive measurements of the height:

$$v_i = \left(\frac{\Delta h}{\Delta t}\right)_i = \frac{h_{i+1} - h_i}{t_{i+1} - t_i}, \quad (1)$$

where the height corresponding to a given instantaneous speed $v_i$ is $h = (h_i + h_{i+1})/2$.

In addition to taking into account the accuracy of the measurements of different values, several additional criteria are adopted to increase the reliability of the obtained results. In order to avoid false peaks in the plots even after smoothing the data, we assume that a deviation from the height and speed distributions is only valid if variations noticed on the plots last longer than two consecutive frames ($\geqslant$15 minutes). The process is accompanied by a visual inspection of eruption images to exclude the possibility of influences from minor internal plasma movements in a prominence loop, or twisting or horizontal movements of the filament body.

As an example of the described procedure we show height–time $h(t)$ and speed–time $v(t)$ plots of EP from 2010 August 7 (Figure 1). Formed on August 4 at 03:00 UT as a small quiescent prominence on the western limb, three days later it erupted, ejecting some of its matter into the heliosphere. The prominence rose 220,000 km above the limb, then left the AIA field of view (Figure 2). The mean velocity during the eruption was 16 km s$^{-1}$.

## 3. Results

We investigate the behavior during eruption of 41 prominences. A full list that includes their characteristics and information about associated events is listed in Table A1 in the Appendix. The events are not specially selected in the sense that the only criteria applied are that the eruptions were observed on the solar limb and had to have happened in the period 2010–2017 (after launching the SDO mission). The kinematic properties of filaments observed on the disk are not the subject of the current research.

Table A1 contains information about the onset of the measurements with different instruments. Often a prominence may have appeared hours or days earlier, but this study does not cover the period prior to EP activation. We obtained a visual inspection of AIA observations and checked the AR identification of SolarMonitor[1] for ARs in the areas of the EPs: 14/41 (34%) of EPs included in the study are related to an AR, while for the other 27 (66%) such an association is not found. The connection of explored EPs with CMEs is checked using both the SOHO LASCO CME Catalog,[2] presented by Gopalswamy et al. (2009), and the AIA Filament Eruption Catalog (McCauley et al. 2015). From the 41 cases listed here, 71% are CME-related.

The information in the last three columns of Table A1 is determined manually by observations. Separating prominences by their class is related to the type of MIL they lie above—active region prominences (ARP), intermediate prominences (IP, situated between two ARs), quiescent prominences (QP) and polar prominences (PP). Some authors also include the class of transequatorial filaments, but representatives of this

[1] https://solarmonitor.org/
[2] https://cdaw.gsfc.nasa.gov/CME_list/index.html

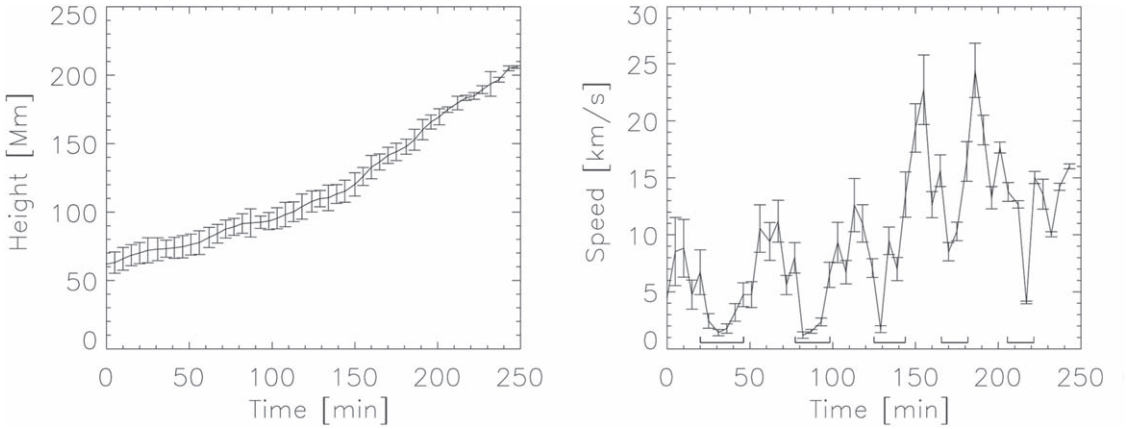


**Figure 1.** Height–time (left) and speed–time (right) plots of the EP from 2010 August 7 after smoothing the data. Time intervals of the observed fluctuations are marked on the speed–time plot with horizontal segments below the curve.

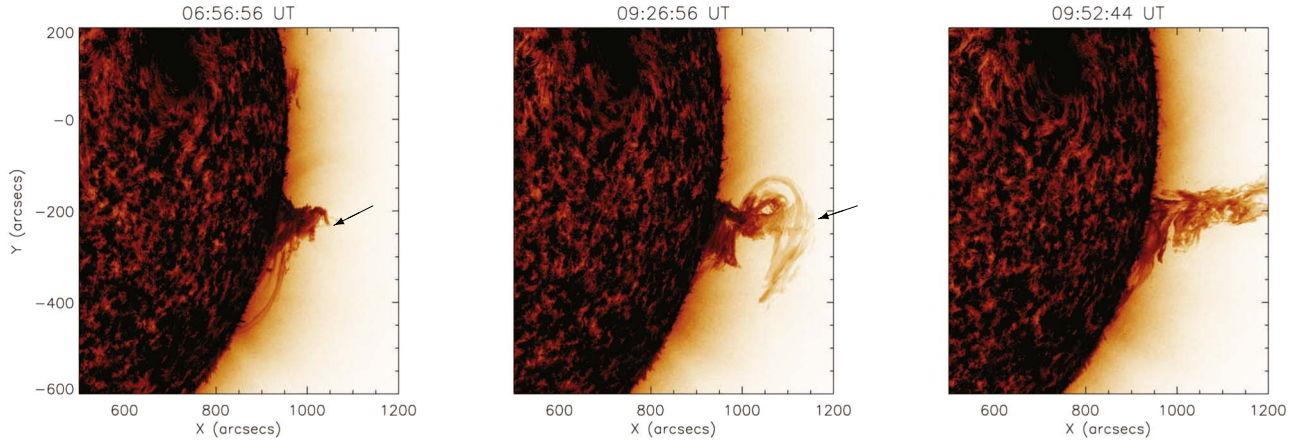


**Figure 2.** The EP from 2010 August 7 as observed from AIA 304 Å. The arrows indicate the fragment of the prominence whose height was measured (left and middle panels). The right panel shows the EP after its edge left the AIA field of view, which marks the end of the measurements.

class are not included in our sample. The event list consists of 20% ARP (8/41), 17 QP (41%), 15% or 6 cases of IP and 24% (10/41) PP. Although some researchers use the term "polar prominences" about structures observed on the boundaries of coronal holes, in this paper the criteria from McCauley et al. (2015) are adopted to conceive a filament as a PP if it is registered at latitudes >50°. All other nonpolar prominences are assumed as midlatitude prominences (observed below 50°). The ratio between the two groups in the explored sample is 76%–24% as the midlatitude filaments are more common.

The EP type (symmetric or asymmetric) is determined according to its geometry. The two groups are almost equally presented, although the asymmetric ones are slightly more frequent (46%–54%). On the other hand, the eruption type (full, partial, or confined) is established by the amount of prominence plasma that escapes the Sun during the eruption. Our list includes 37% full and 37% partial eruptions completed by 11 cases of confined ones (26%).

Dividing the filaments into different categories is summarized in Table 1.

The current study presents velocity variations of the rising prominence plasma during eruption. Similar oscillations are observed in CMEs (Krall et al. 2001; Moon et al. 2004; Shanmugaraju et al. 2010), but never reported for EPs. Krall et al. (2001) and Moon et al. (2004) used smaller samples of events (<20), but Shanmugaraju et al. (2010) explored 116 CMEs, detecting oscillations in 15 cases and explained their origin in the scope of the flux-rope model. The registered periods vary between 48 and 240 minutes.

The procedure described in Section 2 is applied to the full list of 41 EPs. After smoothing the kinematic curves, fluctuations cannot be unambiguously identified in seven cases. On the kinematic profiles of the other 14 EPs, fluctuations in velocity distribution are noted, but they occur once for the entire eruption and the interval between them cannot be established. There are 20 cases where fluctuations are observed more than once during the eruption and allow additional measurements. Therefore, these 20 EPs have been selected as the main subject of this study. They include 3 ARP, 1 IP, 10 QP, and 6 PP. A list of these events and information about observed fluctuations are summarized in Table 2.

Another example is shown on Figure 3—height–time $h(t)$ and speed–time $v(t)$ plots of the EP No. 21 from Table 2. The graphs cover the second eruption of the EP from 2011 May 31 because another activation happened a day earlier. The first eruption continued for less than 60 minutes and only one fluctuation was registered. The second eruption lasted longer (almost 4 hr) until the prominence reached $h_{max} = 270 \times 10^3$ km. The average velocity for the whole eruption is estimated to be 11 km s$^{-1}$ and is marked with a straight line on the plots.

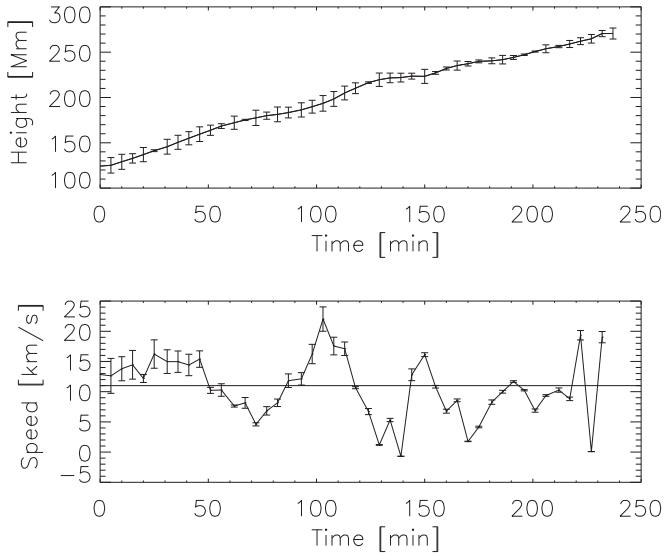


**Figure 3.** Height–time $h(t)$ (upper panel) and speed–time $v(t)$ (lower panel) graphs for the EP from 2011 May 31. The straight line marks the average speed $v_{avg}$.

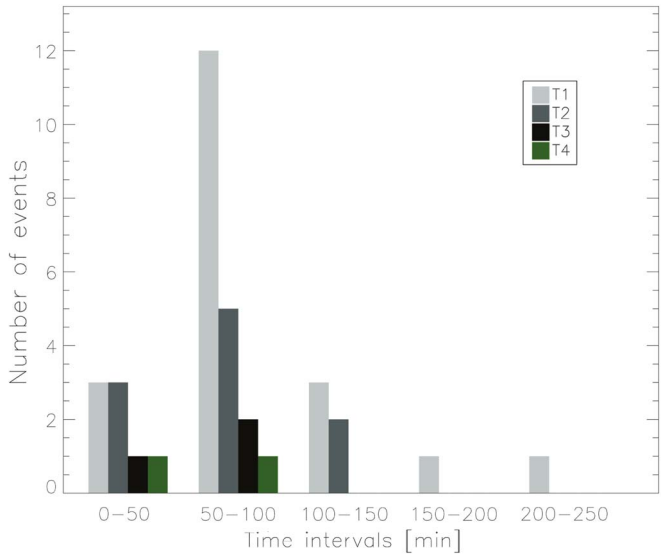


**Figure 4.** Distribution of the time intervals between the fluctuations according to their duration ($T_1$—time between the first and the second fluctuation of different EPs, $T_2$—time between the second and the third variation of EPs, etc.).

**Table 1**
Summary of the Separation of Explored EPs into Different Categories

| Characteristics | Categories | Prominence Classes | | | | |
|---|---|---|---|---|---|---|
| | | All | ARP | IP | QP | PP |
| Associated ARs | Yes | 14 | 8 | 6 | 0 | 0 |
| | No | 27 | 0 | 0 | 17 | 10 |
| CMEs | Yes | 29 | 5 | 5 | 12 | 7 |
| | No | 12 | 3 | 1 | 5 | 3 |
| Location | MLP | 31 | 8 | 6 | 17 | 0 |
| | PCP | 10 | 0 | 0 | 0 | 10 |
| Symmetry | Symmetric | 19 | 4 | 5 | 6 | 4 |
| | Asymmetric | 22 | 4 | 1 | 11 | 6 |
| Eruption type | Full | 15 | 3 | 4 | 6 | 2 |
| | Partial | 15 | 2 | 1 | 6 | 6 |
| | Confined | 11 | 3 | 1 | 5 | 2 |
| LASCO visibility | C2 only | 3 | 0 | 1 | 2 | 0 |
| | C2 and C3 | 7 | 2 | 0 | 4 | 1 |

The time between the first and last height measurements in the AIA field of view $\Delta t$ is given in column 3. Sometimes, the prominence may continue to rise after the top of the loop leaves the field of view of the telescope, but this does not reflect on the value of $\Delta t$. Different EPs show different number of fluctuations—most of them (five) are registered with prominences Nos. 1 and 14 (2010 August 7 and 2011 February 6, respectively), four are the peaks in two other cases (EPs Nos. 4 and 12). The other 16 events show two or three variations. The time intervals between two consecutive minima of the fluctuations are calculated ($T_k$, $1 \leqslant k \leqslant 4$) in minutes and the heights they are registered on ($H_l$, $1 \leqslant l \leqslant 5$) in Mm. The maximum height reached by the EPs in the AIA field of view $h_{max}$ (also in Mm) and the average speed of the EPs during eruption $v_{avg}$ (in km s$^{-1}$) are also estimated.

Measured time intervals between the fluctuations do not show periodicity. The values lie in the range 31–244 minutes and the increase of the intervals in height, typical for CMEs (Shanmugaraju et al. 2010), is observed in only three cases. The explored sample of EPs shows that the most frequent duration of the time between fluctuations is 50–100 minutes, but also durations <50 minutes or 100–150 minutes are often detected (Figure 4). Longer intervals are rather sporadic. For two of the seven prominences that do not show velocity variations, the eruption lasts less than 31 minutes ($\Delta T < T_{min}$), which makes them inappropriate indicators of the presence of the explored fluctuations.

The heights at which variations occur (where the local minimum of the speed is reached) also vary. The values lie in the range 55,000–296,000 km. Often the first deviations occur at heights between 50,000 and 100,000 km, but they can also be expected between 100,000 and 200,000 km. The following fluctuations (second, third, and fourth) tend to happen at altitudes of 100,000–150,000 km (Figure 5). There is a strong correlation between the maximum reached height by the EPs, $h_{max}$, and the heights at which fluctuations are registered, $H_l$ (Figure 6). The Pearson product moment correlation coefficient ($r$) is estimated for the different $H_l$ (plotted with different symbols on the graph): $r_1 = 0.80$; $r_2 = 0.75$; $r_3 = 0.75$. The fourth and fifth heights ($H_4$ and $H_5$) are not included, since only a few EPs reach the fourth and fifth fluctuations and the small number of values will give insignificant results.

A look at the average velocities shows that oscillating EPs are not among the fastest ones ($4 \leqslant v_{avg} \leqslant 55$ km s$^{-1}$); 95% of EPs that exhibit velocity variations have $v_{avg} < 30$ km s$^{-1}$. Only a single EP (No. 17 in Table 2) reaches an average velocity $v_{avg} > 50$ km s$^{-1}$, despite the fact that the comparison with the whole sample of explored EPs shows that the selected 20 are not an exception from the general statistics—only 24% of all prominences included in the study show velocities $v_{avg} > 30$ km s$^{-1}$. It is probably due to the fact that most of the eruptions include an activation phase with a typical speed 1–10 km s$^{-1}$ (Vrsnak 1998; Sterling & Moore 2003, 2004). The results also match with the boundary defined by Hurlburt (2015) of $v_{avg} < 100$ km s$^{-1}$.

**Table 2**
List of EPs that Allow Measurements of the Time and Height Intervals between Two Consecutive Fluctuations

| No. | Date yy mm dd | $\Delta t$ (minutes) | Time Intervals (minutes) | | | | Deceleration Heights (Mm) | | | | | $v_{avg}$ (km s$^{-1}$) | $h_{max}$ (Mm) |
|---|---|---|---|---|---|---|---|---|---|---|---|---|---|
| | | | $T_1$ | $T_2$ | $T_3$ | $T_4$ | $H_1$ | $H_2$ | $H_3$ | $H_4$ | $H_5$ | | |
| 1 | 2010 Aug 7 | 253 | 57 | 51 | 37 | 41 | 74 | 93 | 115 | 146 | 185 | 10 | 220 |
| 2 | 2010 Aug 12–13 | 438 | 244 | | | | 145 | 256 | | | | 9 | 341 |
| 4 | 2010 Aug 27–28 | 420 | 114 | 88 | 83 | | 85 | 97 | 103 | 113 | | 4 | 130 |
| 6 | 2010 Sep 12 | 79 | 58 | | | | 68 | 135 | | | | 13 | 142 |
| 11 | 2011 Jan 25 | 182 | 82 | | | | 122 | 213 | | | | 21 | 330 |
| 12 | 2011 Jan 28 | 222 | 46 | 57 | 73 | | 148 | 159 | 180 | 245 | | 13 | 322 |
| 13 | 2011 Feb 4 | 243 | 41 | 93 | | | 102 | 107 | 126 | | | 4 | 139 |
| 14 | 2011 Feb 6 | 483 | 52 | 114 | 51 | 62 | 95 | 102 | 136 | 150 | 164 | 5 | 175 |
| 16 | 2011 Feb 25 | 82 | 46 | | | | 89 | 130 | | | | 19 | 177 |
| 17 | 2011 Mar 7a | 69 | 53 | | | | 143 | 296 | | | | 55 | 317 |
| 21 | 2011 May 31 | 237 | 67 | 31 | | | 179 | 223 | 239 | | | 11 | 270 |
| 22 | 2011 Jun 5 | 227 | 140 | | | | 182 | 281 | | | | 14 | 342 |
| 23 | 2011 Jun 6 | 291 | 65 | | | | 153 | 152 | | | | 16 | 377 |
| 24 | 2011 Jun 11 | 341 | 57 | 129 | | | 102 | 114 | 173 | | | 9 | 227 |
| 26 | 2012 Jul 28–29 | 513 | 186 | 73 | | | 132 | 162 | 189 | | | 10 | 380 |
| 27 | 2012 Oct 7 | 165 | 51 | 31 | | | 93 | 109 | 125 | | | 7 | 157 |
| 28 | 2013 Feb 27 | 249 | 119 | | | | 144 | 171 | | | | 9 | 274 |
| 31 | 2014 Mar 24 | 109 | 68 | | | | 65 | 109 | | | | 11 | 127 |
| 35 | 2015 Apr 12–13 | 181 | 67 | 31 | | | 55 | 81 | 101 | | | 11 | 161 |
| 40 | 2016 Jul 29 | 149 | 57 | | | | 95 | 62 | | | | 11 | 100 |

**Note.** The numbering of the EPs is taken from Table A1 in the Appendix.

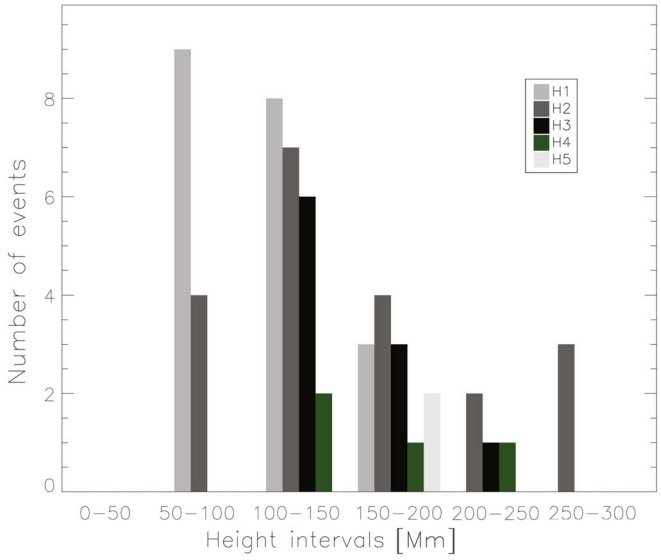


**Figure 5.** Distribution of the intervals between the fluctuations according to the deceleration height at which they occur ($H_1$—the height of the EP at which the first fluctuation occurs, $H_2$—the height of the EP at which the second fluctuation occurs, etc.).

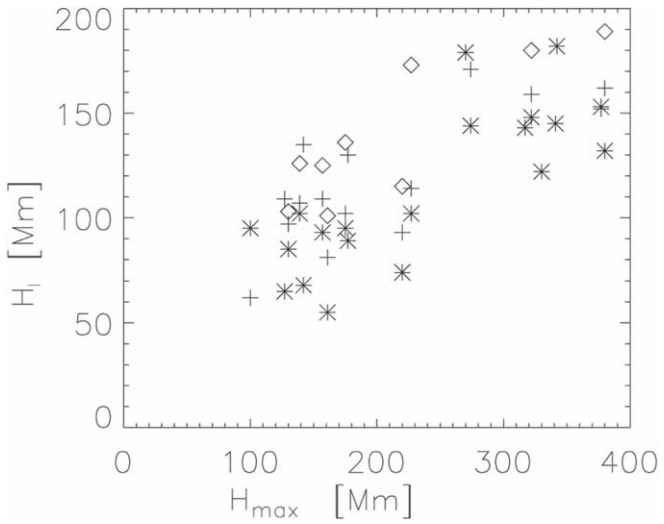


**Figure 6.** The relationship between the maximum height of EPs, $h_{max}$, and the deceleration heights at which velocity variations are detected $H_l$ ($1 \leqslant l \leqslant 3$). Different symbols note the first $H_1$ (starlet), the second $H_2$ (cross), and the third $H_3$ (rhombus) fluctuations of the velocity.

Often the filament eruption continues after the loop leaves the field of view of the AIA. The rising of the prominence up to 30 $R_\odot$ could then be tracked using LASCO data. From our list of selected 20 EPs, only three reach altitudes high enough to be seen by LASCO (EPs Nos. 23, 26, and 28). In addition, seven more EPs that show only one fluctuation in the AIA field of view are also visible by LASCO. We investigated the plots of all these 10 events using the StereoCat tool. EPs on higher altitudes do not show similar behavior closer to the solar limb —fluctuations similar to these observed by AIA cannot be noticed. The height–time dependence is close to linear for all 10 EPs observed by SOHO.

## 4. Discussion and Conclusions

The current study presents a report on the presence of quasiperiodic fluctuations in the instantaneous velocities of eruptive prominences. The explored events reach heights in the range 100–380 Mm in the AIA field of view and 4.4–22.8 $R_\odot$ observed by LASCO. We determine delays in the speed of the plasma of the highest prominence fragments in the AIA/SDO field of view.

To perform an accurate measurement, an IDL procedure is created that ensures the the EP and background components are precisely distinguished between in the signal profile. Thus, the selection of the highest fragment of an EP is assured, since the top parts of filament arches are usually fainter due to a lower density of the plasma.

After analyzing the height–time and speed–time plots of 41 EPs using AIA/SDO data, velocity fluctuations of the rising prominence material are detected in 34 cases (83%). Similar variations, but observed for propagation of CMEs, are previously reported (Krall et al. 2001; Moon et al. 2004; Shanmugaraju et al. 2010). They are rarer when observed on CMEs—15/116 cases detected by Shanmugaraju et al. (2010).

More than a single variation for the period of the eruption is detected in 20/40 EPs, which allows measurement of the time intervals between fluctuations. A periodicity could not be found as time intervals lie in the range 31–244 minutes. The most frequent intervals are those with a duration between 50–100 minutes. The heights at which fluctuations are observed vary between 55,000–296,000 km. The first variation happens usually in the range 50,000–100,000 km and the following ones between 100,000–150,000 km.

Generally such a deviations could be caused not only by delays in the ascent of EPs, but also from changes in the plasma distribution in different fragments of the prominence body, relative movements of fibers or small-scale arches that form the EP, twists, writhes, etc. That is why our sample of events consists of various EPs with different structures, environments and helicity. This variety is visible from a comparison of eight from the selected 20 EPs (listed in Table 2) that are included in the AIA Filament Eruption Catalog (McCauley et al. 2015), where information about the EP type, symmetry, twists, writhes, and environment is provided. To check the hypothesis of whether the subject of the observed fluctuations is only the upper part of an EP or the whole body, we performed a measurement of a lower segment of a few random filaments where tracking of the same structure during the essential part of the eruption is possible. Finally, we realized that fluctuations are noticeable also in other segments of the EPs and their peaks are registered a bit earlier, since the selected parts of the skeletons are situated lower than the leading edges.

Fluctuations are not detected when analyzing the behavior of 10 EPs that can be tracked at higher altitudes in LASCO/SOHO C2 and C3 fields of view. This fact perhaps gives a hint for the origin of the fluctuations. The magnetic field plays a primary role in filament formation, stability, and eruption (Su & van Ballegooijen 2012). But the ascending prominence plasma passes various coronal magnetic structures that may affect its propagation. The interaction between prominence material frozen in the magnetic structures and surrounding magnetic arcades may cause fluctuations of the velocity.

Often during eruptions, one can notice how the top of a prominence loop is being flattened and thus tracks the boundaries of a part of the large-scale coronal structure consisting of a prominence and a cavity (Berger 2012). The onset of the eruptive phase marks the occurrence of a large-scale magnetic reconnection (Joshi et al. 2016). This moment may be representing the passage of prominence material through coronal cavities, and is characterized by an increase in the rising velocity with 20–40 km $s^{-1}$. The question about the relationship between prominences and coronal cavities is still not unconditionally answered. Although the opinion that all filaments are surrounded by cavities is quite widespread, it is assumed that observations of prominences without a cavity around them is due to projection effects by foreground coronal arcade emission (Gibson et al. 2010). The environmental magnetic structures causing the variations are more common at heights $<2\,R_{\odot}$ above the solar limb. That is why the velocity increase continues above cavities in the LASCO field of view (at altitudes $>2\,R_{\odot}$) when the prominence loop reaches a free acceleration region passing through open magnetic structures in the corona (Fisk 2005; Gilbert et al. 2007b) without exhibiting fluctuations. It is important to notice that the behavior of prominences in the region 0.6–2 $R_{\odot}$ still remains unexplored, since it covers the gap between the the AIA and LASCO C2 fields of view.

This work was partially supported by the Bulgarian Ministry of Education and Science under the National Research Programme "Young scientists and postdoctoral students" approved by DCM #577/17.08.2018 and by the National Science Fund of Bulgaria with contract Nos. KP-06-H28/4 and KP-06-M38/3.

*Facilities:* SDO(AIA), SOHO(LASCO).

*Software:* SolarSoftware (Bentely & Freeland 1998).

## Appendix
## Eruptive Prominences List

Detailed information about the explored eruptive prominences and associated phenomena is given below in Table A1.

**Table A1**
Details About the Explored EPs and Associated Active Processes: Associated ARs, CMEs (First Appearance in the LASCO/SOHO Field of View, Linear Speed *v*)

| No. | Date | Onset (UT) | | | ARs | CMEs | | Class | EP | Eruption |
|---|---|---|---|---|---|---|---|---|---|---|
| | yyyy mm dd | AIA | C2 | C3 | | Onset (UT) | *v* (km $s^{-1}$) | | Type | Type |
| 1 | 2010 Aug 7 | 06:00 | | | No | 11:00 | 228 | QP | A | P |
| 2 | 2010 Aug 12–13 | 23:00 | | | No | No | | QP | A | F |
| 3 | 2010 Aug 25 | 01:00 | | | No | No | | PP | A | P |
| 4 | 2010 Aug 27–28 | 23:00 | | | No | 11:12 | 124 | PP | S | C |
| 5 | 2010 Sep 10 | 12:00 | | | No | 12:24 | 295 | PP | S | F |
| 6 | 2010 Sep 12 | 05:50 | | | No | No | | PP | S | C |
| 7 | 2010 Sep 30 | 18:30 | 01:25 | 03:30 | No | 23:05 | 399 | QP | A | F |
| 8 | 2011 Jan 22a | 11:00 | | | No | No | | QP | S | P |
| 9 | 2011 Jan 22b | 21:00 | 01:48 | | No | 00:48 | 448 | QP | S | F |
| 10 | 2011 Jan 24 | 00:00 | 04:48 | 08:06 | No | 02:00 | 258 | PP | A | P |
| 11 | 2011 Jan 25 | 02:00 | | | No | No | | QP | A | P |

**Table A1**
(Continued)

| No. | Date | Onset (UT) | | | ARs | CMEs | | Class | EP | Eruption |
|---|---|---|---|---|---|---|---|---|---|---|
| | yyyy mm dd | AIA | C2 | C3 | | Onset (UT) | $v$ (km s$^{-1}$) | | Type | Type |
| 12 | 2011 Jan 28 | 00:00 | | | No | 05:00 | 170 | QP | S | P |
| 13 | 2011 Feb 4 | 15:00 | | | No | 20:00 | 192 | QP | S | C |
| 14 | 2011 Feb 6 | 00:00 | | | No | No | | QP | A | C |
| 15 | 2011 Feb 23–24 | 21:00 | | | No | 00:48 | 51 | QP | A | C |
| 16 | 2011 Feb 25 | 16:30 | | | No | No | | PP | A | P |
| 17 | 2011 Mar 7a | 15:15 | | | 11164 | No | | ARP | A | F |
| 18 | 2011 Mar 7b | 19:45 | 20:24 | 21:18 | No | 20:00 | 2125 | ARP | A | F |
| 19 | 2011 Mar 20 | 15:00 | | | No | No | | QP | A | C |
| 20 | 2011 May 30 | 09:00 | | | No | 10:00 | 299 | QP | A | F |
| 21 | 2011 May 31 | 10:00 | | | No | 14:12 | 278 | QP | A | P |
| 22 | 2011 Jun 5 | 11:30 | | | No | 16:59 | 207 | QP | A | C |
| 23 | 2011 Jun 6 | 03:00 | 08:29 | 10:35 | No | 07:30 | 582 | PP | S | P |
| 24 | 2011 Jun 11 | 16:30 | | | No | 19:47 | 449 | PP | A | P |
| 25 | 2012 Mar 4 | 11:15 | | | 11429 | 11:00 | 1306 | ARP | S | C |
| 26 | 2012 Jul 28–29 | 15:30 | 01:25 | | No | 23:48 | 460 | QP | A | P |
| 27 | 2012 Oct 7 | 03:00 | | | No | 07:36 | 564 | PP | A | F |
| 28 | 2013 Feb 27 | 00:00 | 05:30 | 06:42 | No | 04:00 | 622 | QP | S | F |
| 29 | 2013 Apr 19 | 14:00 | | | No | 16:48 | 266 | PP | A | P |
| 30 | 2014 Feb 11 | 18:40 | | | 11972<br>11975 | 19:24 | 613 | IP | S | F |
| 31 | 2014 Mar 24 | 05:00 | | | 12004 | 07:12 | 809 | ARP | A | P |
| 32 | 2014 Nov 1 | 04:00 | 05:24 | | 12200<br>12201 | No | | IP | S | F |
| 33 | 2014 Nov 9 | 09:00 | | | 12207<br>12208 | 10:24 | 633 | IP | S | P |
| 34 | 2015 Feb 21 | 09:20 | 10:12 | 11:18 | No | 09:24 | 1120 | QP | S | F |
| 35 | 2015 Apr 12–13 | 22:00 | | | 12318<br>12320 | 23:48 | 678 | IP | A | C |
| 36 | 2015 May 12 | 02:00 | | | 12335<br>12337 | 02:48 | 772 | IP | S | F |
| 37 | 2015 Jun 18 | 00:30 | | | 12365<br>12368 | 01:26 | 1714 | IP | S | F |
| 38 | 2015 Jul 19 | 08:00 | 10:12 | 11:18 | 12384 | 09:48 | 782 | ARP | S | F |
| 39 | 2016 Jun 25 | 02:00 | | | Small AR | 02:48 | 540 | ARP | A | P |
| 40 | 2016 Jul 29 | 07:00 | | | 12569 | No | | ARP | S | C |
| 41 | 2017 Jan 2 | 08:00 | | | 12622 | No | | ARP | S | C |

**Note.** Abbreviations: ARs—active regions, CMEs—coronal mass ejections, $v$—velocity, QP—quiescent prominence, PP—polar prominence, S—symmetric (prominence), P—partial (eruption), F—full (eruption).

## ORCID iDs

Tsvetan Tsvetkov https://orcid.org/0000-0002-5838-5244

## References

Babcock, H. W., & Babcock, H. D. 1955, ApJ, 121, 349
Bentely, R. D., & Freeland, S. L. 1998, in ESA Special Publication, Vol. 417, Crossroads for European Solar and Heliospheric Physics. Recent Achievements and Future Mission Possibilities (Paris: ESA), 225
Berger, T. 2012, in ASP Conf. Ser. 463, Second ATST-EAST Meeting: Magnetic Fields from the Photosphere to the Corona, ed. T. R. Rimmele et al. (San Francisco, CA: ASP), 147
Domingo, V., Fleck, B., & Poland, A. I. 1995, SoPh, 162, 1
Fisk, L. A. 2005, ApJ, 626, 563
Gibson, S. E., Kucera, T. A., Rastawicki, D., et al. 2010, ApJ, 724, 1133
Gilbert, H., Kilper, G., & Alexander, D. 2007a, ApJ, 671, 978
Gilbert, H. R., Alexander, D., & Liu, R. 2007b, SoPh, 245, 287
Gilbert, H. R., Holzer, T. E., Burkepile, J. T., & Hundhausen, A. J. 2000, ApJ, 537, 503
Gopalswamy, N., Yashiro, S., Michalek, G., et al. 2009, EM&P, 104, 295
Hurlburt, N. 2015, JSWSC, 5, A39
Joshi, B., Kushwaha, U., Veronig, A. M., & Cho, K.-S. 2016, ApJ, 832, 130
Krall, J., Chen, J., Duffin, R. T., Howard, R. A., & Thompson, B. J. 2001, ApJ, 562, 1045
Lemen, J. R., Title, A. M., Akin, D. J., et al. 2012, SoPh, 275, 17
Mackay, D. H., Gaizauskas, V., & Yeates, A. R. 2008, SoPh, 248, 51
McCauley, P. I., Su, Y. N., Schanche, N., et al. 2015, SoPh, 290, 1703
Moon, Y.-J., Cho, K. S., Smith, Z., et al. 2004, ApJ, 615, 1011
Pesnell, W. D., Thompson, B. J., & Chamberlin, P. C. 2012, SoPh, 275, 3
Rompolt, B. 1984, AdSpR, 4, 357
Rompolt, B. 1990, HvaOB, 14, 37
Shanmugaraju, A., Moon, Y.-J., Cho, K.-S., et al. 2010, ApJ, 708, 450
Sterling, A. C., & Moore, R. L. 2003, ApJ, 599, 1418
Sterling, A. C., & Moore, R. L. 2004, ApJ, 613, 1221
Su, Y., & van Ballegooijen, A. 2012, ApJ, 757, 168
Vrsnak, B. 1998, in ASP Conf. Ser. 150, IAU Coll. 167: New Perspectives on Solar Prominences, ed. D. F. Webb, B. Schmieder, & D. M. Rust (San Francisco, CA: ASP), 302